

1 Solar Flare Effects on 150-km Echoes Observed Over 2 Jicamarca: WACCM-X Simulations

3 **N. M. Pedatella^{1,2}, J. L. Chau³, J. Vierinen⁴, L. Qian¹, P. Reyes⁵, E. Kudeki⁶,
4 G. Lehmacher⁷, and M. Oppenheim⁸**

5 ¹High Altitude Observatory, National Center for Atmospheric Research, Boulder, CO, USA.

6 ²COSMIC Program Office, University Center for Atmospheric Research, Boulder, CO, USA.

7 ³Leibniz Institute of Atmospheric Physics, Rostock University, Kühlungsborn, Germany.

8 ⁴Department of Physics and Technology, University of Tromsø, Tromsø, Norway

9 ⁵Center for Geospace Studies, SRI International, Menlo Park, California, USA

10 ⁶Department of Electrical and Computer Engineering, University of Illinois at Urbana-Champaign,

11 ⁷Department of Physics and Astronomy, University of Clemson, Clemson, SC, USA.

12 ⁸Center for Space Physics, Boston University, Boston, MA, USA.

13 Key Points:

- 14 • There is a good agreement between observed morphology of 150-km echoes and
15 simulated electron densities during a solar flare.
- 16 • The results support the hypothesis that layering of 150-km echoes is connected
17 to electron densities.
- 18 • Decrease in vertical plasma drift during the solar flare can be attributed to changes
19 in E-region conductivity.

20 **Abstract**

21 Jicamarca Radio Observatory observations and Whole Atmosphere Community Climate
 22 Model with thermosphere-ionosphere eXtension (WACCM-X) simulations are used to
 23 investigate the effects of the September 7, 2005 X-17 solar flare on 150-km echoes, elec-
 24 tron densities, and vertical plasma drifts. The solar flare produces a remarkably simi-
 25 lar response in the observed 150-km echoes and simulated electron densities. The results
 26 provide additional evidence of the relationship between the background electron density
 27 and the layering structure that is seen in 150-km echoes. The simulations also capture
 28 a similar rapid decrease in vertical plasma drift velocity that is seen in the observations.
 29 The simulated change in vertical plasma drift is, however, weaker than the observed de-
 30 crease at the longitude of Jicamarca, though it is stronger east of Jicamarca. The effect
 31 of the solar flare on the vertical plasma drifts is attributed to changes in conductivity
 32 due to the enhanced ionization during the solar flare.

33 **1 Introduction**

34 Despite being first observed over 50-years ago (Balsley, 1964), the source of the en-
 35 hanced VHF radar echoes that are observed near 150 km remains unexplained. These
 36 so-called 150-km echoes have subsequently been observed in the equatorial ionosphere
 37 at multiple longitudinal locations (J. L. Chau & Kudeki, 2006; Kudeki et al., 1998; de
 38 Paula & Hysell, 2004; Tsunoda & Ecklund, 2008; Choudhary et al., 2004; A. K. Patra
 39 et al., 2008). The 150-km echoes are observed nearly every day, and they are thus a ubiq-
 40 uitous feature of the equatorial ionosphere. The characteristics of the 150-km echoes have
 41 been well documented by observations. These characteristics include their occurrence
 42 only during the daytime, a necklace-like shape with descending structures prior to noon
 43 and ascending structures after noon, as well as the formation of distinct layers. More-
 44 over, the majority of 150-km echoes are a manifestation of naturally enhanced incoher-
 45 ent scatter echoes (e.g., J. L. Chau, 2004; J. Chau et al., 2009; J. L. Chau & Kudeki, 2013).
 46 Some of these features have led to the hypothesis that the 150-km echoes are due to pho-
 47 toelectrons (e.g., Oppenheim & Dimant, 2016). The connection to photoelectrons is fur-
 48 ther supported by the absence of 150-km echoes during the January 2010 solar eclipse
 49 (A. K. Patra et al., 2011), as well as their modification by solar flares (Reyes, 2012).

50 The photoelectron origin of the 150-km echoes cannot fully explain the formation
 51 of several distinct layers. There does, however, appear to be a connection between the
 52 electron density, the temporal and altitudinal structure of the layers, and the gaps that
 53 form between layers (e.g., J. L. Chau et al., 2009; Reyes, 2017). For example, Reyes (2017)
 54 show a close correspondence between short-period (~5-10 minute) fluctuations in elec-
 55 tron densities and the gaps in the 150-km echoes. This has led to the suggestion that
 56 the gaps between layers may form at distinct plasma frequencies (e.g., G. Lehmacher et
 57 al., 2018). However, A. Patra et al. (2017) recently disputed the connection between pho-
 58 toelectrons and 150-km echoes. They found an inverse relationship between 150-km echo
 59 power and EUV flux, and hypothesized that neutral dynamics play an important role
 60 in the formation of 150-km echoes. Though neutral dynamics may contribute to the 150-
 61 km echoes, they would not fully explain features such as the daytime only occurrence,
 62 narrow spectral widths, solar eclipse, and solar flare effects. These features suggest that
 63 photoelectrons contribute to the formation of 150-km echoes.

64 Nonetheless, the connection between 150-km echoes, photoelectrons, and electron
 65 densities has yet to be fully explored. Understanding the relationship between 150-km
 66 echoes and electron densities would provide an additional step towards developing a com-
 67 plete theory to explain the 150-km echoes, improving our understanding of the equato-
 68 rial ionosphere. If a relationship between electron density and the power striations can
 69 be determined, 150-km echoes could also provide a high signal-to-noise ratio radar tar-

70 get for accurately measuring the electron density between the E-region and the F-region
 71 of the ionosphere.

72 The main objective of the present study is to further investigate the connection be-
 73 tween electron densities and the 150-km echo layers. This is done through a compari-
 74 son of Jicamarca Radio Observatory (JRO) observations of 150-km echoes during the
 75 September 7, 2005 solar flare with electron densities simulated in the Whole Atmosphere
 76 Community Climate Model with thermosphere-ionosphere eXtension (WACCM-X). The
 77 simulated electron densities closely follow the observed layering structure of the 150-km
 78 echoes, supporting the close connection between the electron densities and the gaps that
 79 form between the 150-km echo layers. We further investigate the change in vertical plasma
 80 drift velocity during the solar flare, and find that this is likely related to a rapid change
 81 in the conductivity that occurs during the solar flare.

82 **2 JRO Observations**

83 The JRO observations were taken as part of a MST-ISR experiment, which is an
 84 experiment designed to observe the Mesosphere, Stratosphere and Troposphere (MST)
 85 at the same time as the ionosphere in quasi thermal equilibrium via the Incoherent Scat-
 86 ter Radar (ISR) mode (e.g., G. A. Lehmacher et al., 2009, 2019). The MST mode allows
 87 the observation from 0 km to 200 km, while the ISR mode measures from 200 km to 900
 88 km in altitude. Although the mesosphere stops at around 100 km, the MST mode has
 89 proven to also be useful in the study of coherent scattering from ionospheric irregular-
 90 ities, such as those coming from 150-km echoes (e.g., Kudeki & Fawcett, 1993; J. L. Chau
 91 & Kudeki, 2006). The MST-ISR mode is realized by interleaving sequences of pulses with
 92 different repetition, pulse width and pulse coding. In the case of the MST part, 20 con-
 93secutive pulses with 1.33 ms (or \sim 200 km) interpulse period (IPP) and 64 baud com-
 94plementary codes pulses with a total width of 64 μ s (or 9.6 km) are transmitted. In the
 95 case of the ISR part, 2 Barker-3 coded pulses with a total width of 300 μ s (or 45 km)
 96 and an IPP of 6.66 ms (or \sim 1000 km) were transmitted.

97 These pulse sequences were transmitted simultaneously on four different beam po-
 98 sitions (North, East, South and West), taking advantage of the modular and polariza-
 99 tion features of JRO. Two transmitters of 1 MW peak power each, were combined be-
 100 fore feeding all four beams simultaneously, i.e., on each beam 500 kW peak power was
 101 transmitted. In this work we present the results of September 7, 2005 only from the MST
 102 part of the West beam (-87.68° azimuth, 87.52° elevation), which is the beam pointing
 103 the closest to perpendicular to the Earth's magnetic field **B** (beam gain peak $\sim 0.8^\circ$ from
 104 perpendicular to **B** and elongated in the North-South direction with a beam width of
 105 $\sim 1.4^\circ$) at 150 km at the time of the experiment. More details of the JRO modes, sig-
 106 nal processing, other solar flare effects, and other events can be found in Reyes (2012).

107 **3 WACCM-X**

108 Model simulations are performed in WACCM-X version 2.0 (H.-L. Liu et al., 2018).
 109 WACCM-X extends from the surface to the upper thermosphere (4.1×10^{-10} hPa, ~ 500 -
 110 700 km depending on solar activity), and has a resolution of 1.9° in latitude, 2.5° in lon-
 111 gitude, and 0.25 scale heights above the stratosphere. Up to the lower thermosphere, WACCM-
 112 X is based on the Community Atmosphere Model (CAM) version 4 (Neale et al., 2013)
 113 and Whole Atmosphere Community Climate Model (WACCM) version 4 (Marsh et al.,
 114 2013). Upper atmospheric processes, including the transport of O^+ , self-consistent iono-
 115 spheric electrodynamics, and energetics included in WACCM-X are primarily based on
 116 the Thermosphere-Ionosphere-Electrodynamics General Circulation Model (TIE-GCM)
 117 (Roble et al., 1988; Richmond et al., 1992). H.-L. Liu et al. (2018) and J. Liu et al. (2018)
 118 provide a detailed description and validation, respectively, of WACCM-X version 2.0

119 For the model simulations in the present study, the specified dynamics approach
 120 (Smith et al., 2017) is used to constrain the lower atmosphere meteorology up to 50 km
 121 to the National Aeronautics and Space Administration (NASA) Modern Era Retrospec-
 122 tive Analysis for Research and Applications version 2 (MERRA-2) (Gelaro et al., 2017).
 123 Geomagnetic forcing is incorporated by imposing the Heelis empirical convection pat-
 124 tern at high latitudes (Heelis et al., 1982), which is driven by the 3-hr geomagnetic K_p
 125 index. The Flare Irradiance Spectral Model (FISM) (Chamberlin et al., 2008) provides
 126 the solar spectral irradiance for the solar flare that occurred on September 7, 2005. FISM
 127 is an empirical model that uses observational data from Geostationary Operational En-
 128 vironmental Satellite (GOES) X-Ray Sensor (XRS), Thermosphere Ionosphere Mesosphere
 129 Energetics and Dynamics (TIMED) Solar Extreme Ultraviolet Experiment (SEE), and
 130 Solar Radiation and Climate Experiment (SORCE) SOLar Stellar Irradiance Compar-
 131 ison Experiment (SOLSTICE) to estimate the solar irradiance at wavelengths from 0.1
 132 to 190 nm at 60 s temporal resolution. FISM is thus able to capture the solar irradiance
 133 variability during solar flares at wavelengths that directly impact the ionosphere and ther-
 134 mosphere, which includes the soft X-rays (0.1-10 nm) and extreme ultraviolet (EUV, 10-
 135 121.6 nm). Previous studies have demonstrated that the solar flare irradiance informa-
 136 tion provided by FISM is suitable for studying the effects of solar flares in the mesosphere,
 137 thermosphere, and ionosphere (e.g., Qian et al., 2011; Pettit et al., 2018).

138 4 Results and Discussion

139 4.1 Flare Impact on 150-km Echoes and Electron Density

140 The signal to noise ratio (SNR) observed by JRO on September 7, 2005 is shown
 141 in Figure 1a. The X-ray flux observed by GOES XRS is shown in Figure 1c. An X-17
 142 solar flare began at 17:17 UT, reached its maximum intensity at 17:40 UT, and the so-
 143 lar irradiance returned to nominal levels over the next \sim 1 hour. Prior to the solar flare,
 144 the characteristic behavior of 150-km echoes is observed, with gradually descending lay-
 145 ers of enhanced SNR that are 5-10 km thick. The enhanced SNR layers are separated
 146 by gaps that are on the order of a kilometer thick. The layers descend rapidly in alti-
 147 tude beginning around 17:30 UT, which corresponds to the start of the solar flare. Af-
 148 ter the flare, around 18:00 UT, the layers initially rise rapidly, though the rate of ascent
 149 slows over the following hour. The vertical thickness of the layers also appears to be changed
 150 by the solar flare, with the layers being narrower following the solar flare.

151 The corresponding electron densities simulated by WACCM-X are shown in Fig-
 152 ure 1b. Note that the WACCM-X results have been shifted later by 5 minutes to be more
 153 consistent with the observations. This corresponds to the model time step, as well as the
 154 solar flare forcing input, so we consider a 5 minute offset to not be a significant discrep-
 155 ancny between the timing of the solar flare effects in the observations and simulations.
 156 We also note that the coarse (relative to solar flare time scales) time step of WACCM-
 157 X may tend to smooth the model response to the solar flare. Contours of constant elec-
 158 tron density in the WACCM-X simulations exhibit many of the same features that are
 159 seen in the observations. Prior to the flare, the electron density contours can be seen to
 160 largely track the gaps and edges in the radar echoes. The exception being the smaller
 161 scale structures that are seen in the observations, which are attributed to gravity waves
 162 that are unresolved in WACCM-X. The consistency between the Jicamarca observations
 163 and WACCM-X simulations is especially apparent during the solar flare. In particular,
 164 both show a rapid descent in altitude beginning around 17:30 UT, followed by a more
 165 gradual ascent around 18:00 UT. The electron density contours are additionally more
 166 closely spaced following the flare, a feature consistent with the JRO SNR observations.

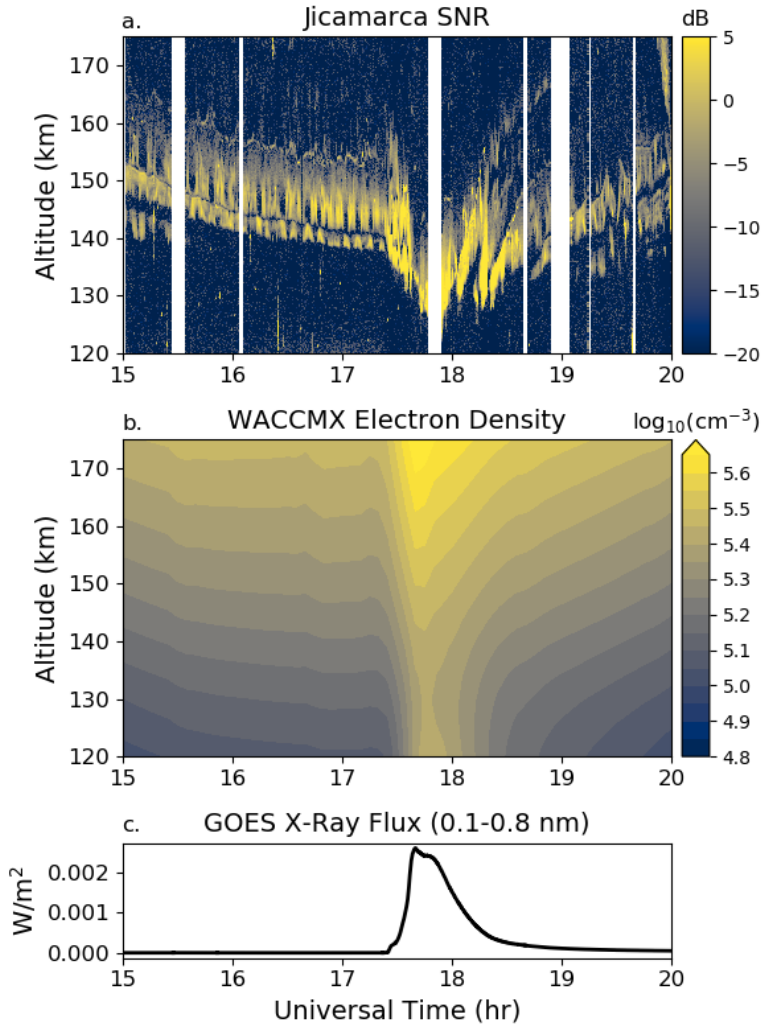


Figure 1. (a) JRO observed signal to noise ratio (SNR) during the September 7, 2005 solar flare. White areas indicate time periods without observations. (b) Electron densities simulated by WACCM-X at the location of Jicamarca, Peru. (c) Observed GOES x-ray flux for 0.1-0.8 nm.

To better illustrate the relationship between the 150-km echoes observed by JRO and the electron density simulated by WACCM-X, the two are plotted together in Figure 2 for a shorter time interval around the solar flare. The remarkable agreement in the effect of the solar flare on contours of constant electron density and the structure of the 150-km echo layers can be clearly seen in Figure 2. From Figure 2, it is apparent that the gaps in the 150-km echoes seem to follow electron density contours; however, the reason for this relationship is not yet known. With plasma-lines, there is a matching condition between plasma-frequency, radar wavelength, and suprathermal electron velocity (photoelectrons and auroral secondary electrons), which results in electron density dependent plasma-line radar echo enhancements (Perkins et al., 1965). The fact that this also occurs for the 150-km echoes, points to a similar wave-particle interaction (Oppenheim & Dimant, 2016). An alternative possibility is that the observed layering is related to gyro-harmonics (G. Lehmacher et al., 2018), though this would not explain the formation of multiple layers in the E-region because there are only two contours in the E-region where the electron density plasma frequency is an integer multiple of the gyro-frequency.

182 Thus, although the results demonstrate a close connection between electron density and
 183 the 150-km echo layers, the reason for this relationship remains unknown. Both of the
 184 previously mentioned hypotheses will be explored in detail in a future work, where com-
 185 parisons between JRO observations and WACCM-X simulations under nominal (i.e., non-
 186 flare) conditions will be considered.

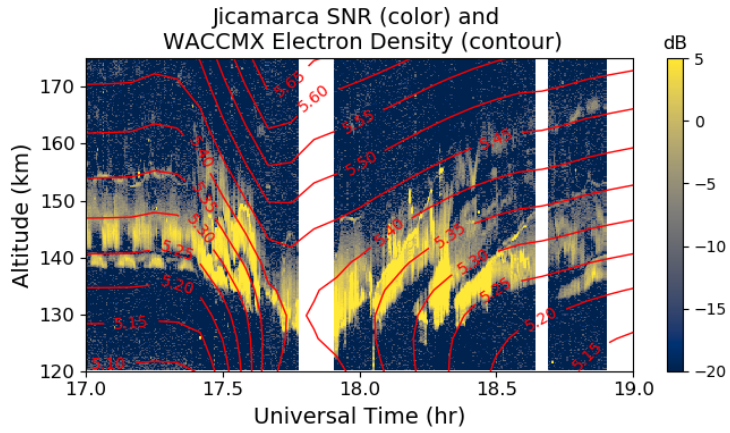


Figure 2. Observed signal to noise ratio (SNR) (colors), and WACCM-X electron densities in units of $\log_{10}\text{cm}^{-3}$ (contours) during the September 7, 2005 solar flare.

187

4.2 Flare Impact on Vertical Plasma Drifts

188

In addition to influencing the E-region electron densities and 150-km echoes, so-
 189 lar flares can modulate the electrodynamics of the ionosphere (Qian et al., 2012; Zhang
 190 et al., 2017). As seen in Figure 3, the JRO observations of vertical plasma drift veloc-
 191 ity (blue) show a clear response to the solar flare, and the drifts exhibit a sudden ~ 15
 192 ms^{-1} decrease at the onset of the solar flare. The WACCM-X simulations only exhibit
 193 a weak ($1\text{-}2 \text{ ms}^{-1}$) response to the solar flare at 285°E geographic longitude (black). How-
 194 ever, a stronger response occurs in the WACCM-X simulations at 320°E geographic lon-
 195 gitude (red), though it is still slightly weaker than seen in the observations. Nonethe-
 196 less, the vertical plasma drift response at 320°E is generally consistent with the JRO ob-
 197 servations, and we can thus use the simulations to understand the mechanism behind
 198 the rapid decrease in the vertical plasma drift during the solar flare.

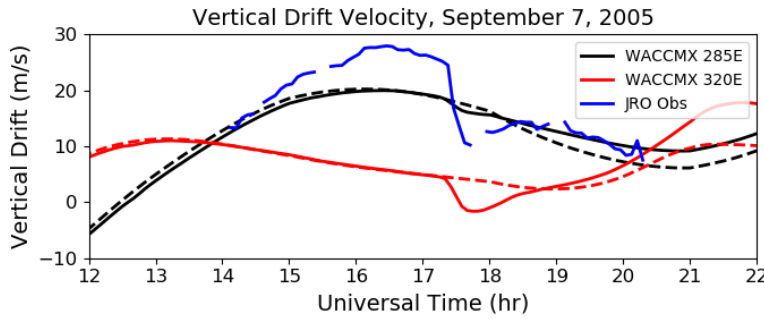


Figure 3. Equatorial vertical drift velocity on September 7, 2005 from Jicamarca 150-km echoes (blue), and WACCM-X simulations at 285°E (black) and 320°E (red) geographic longitude. Dashed lines indicate WACCM-X results without inclusion of the solar flare.

Previous studies investigating the solar flare effects on electrodynamics, and ionospheric currents, have attributed the response to a change in the ionospheric conductivity (Qian et al., 2012; Annadurai et al., 2018) and/or penetration electric field due to the imbalance of high latitude region-1 and region-2 field aligned currents. The later mechanism was proposed by Zhang et al. (2017) as a source of the decrease in vertical plasma drift observed during the September 7, 2005 solar flare. The WACCM-X simulation does not include the effects of penetration electric fields, and we therefore attribute the change in vertical plasma drifts to changes in the ionospheric conductivity. It should be noted that we cannot entirely discount effects of penetration electric fields, and inclusion of penetration electric fields could lead to a larger vertical plasma drift response. The fact that the WACCM-X simulations capture a decrease in vertical plasma drifts at 320°E does, however, indicate that conductivity changes are an important mechanism by which solar flares influence electrodynamics.

The changes in the WACCM-X Hall (σ_H) and Pedersen (σ_P) conductivities at 17:45 UT are shown in Figure 4 for 285°E and 320°E geographic longitude. Note that the changes are calculated relative to a WACCM-X simulation that did not include the solar flare forcing. For reference, maximum Hall and Pedersen conductivities at this time in the WACCM-X simulation without the solar flare are $\sim 8 \times 10^{-4}$ S/m and $\sim 5 \times 10^{-4}$ S/m, respectively. The conductivity changes due to the solar flare are thus large compared to the background conductivities. The corresponding zonal winds are shown in Figures 4c and 4f. Note that the zonal winds are largely unchanged by the solar flare below ~ 175 km, and are enhanced by $5\text{--}10$ ms^{-1} above 200 km (not shown). The change in Hall conductivity due to the flare is larger at 285°E than it is at 320°E, which should contribute to a larger decrease in the daytime eastward electric field, and thus a larger decrease in the vertical drift at 285°E. The change in Pedersen conductivity due to the solar flare is generally similar at the two longitudes. The background zonal winds are, however, notably different which is likely due to the differences in local time at the two longitudes (12:45 SLT at 285°E and 15:05 SLT at 320°E). We therefore attribute the smaller change in the simulated drift response at 285°E to be due to the zonal winds at the time of the solar flare, and it is possible that WACCM-X does not capture the flare effects at 285°E due to deficiencies in the zonal winds. These differences highlight the need to accurately simulate both the neutral winds and conductivities in order to accurately simulate the solar flare effects on ionospheric electrodynamics.

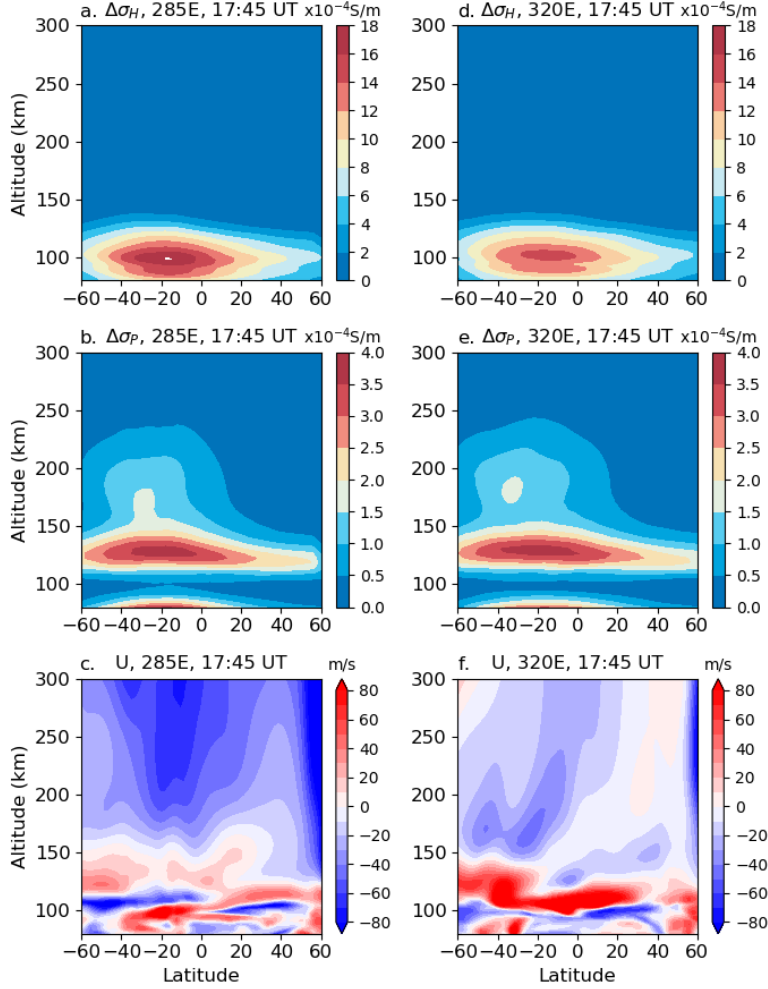


Figure 4. Changes in (a) Hall and (b) Pedersen conductivity at 285° E geographic longitude and 17:45 UT. (c) Zonal wind at 285° geographic longitude and 17:45 UT. (d-f) Same as (a-c) except for at 320° E geographic longitude.

5 Conclusions

The present study investigates the effects of the September 7, 2005 X-17 solar flare on the equatorial ionosphere using a combination of JRO observations and WACCM-X simulations. The solar flare is found to produce similar changes in the layering structure of observed 150-km echoes and simulated electron densities. In particular, both reveal a rapid descent at the onset of the solar flare, followed by a gradual ascent following the solar flare. The 150-km echo layers and contours of constant electron density are also both found to be narrower in vertical extent following the solar flare. These similarities support a connection between the background electron density and the layering structure that is seen in 150-km echoes. The reason for this relationship does, however, remain unknown, and further investigations into this connection will help in understanding the mechanisms that form the still unexplained 150-km echoes. The results also demonstrate that relatively coarse resolution whole atmosphere-ionosphere general circulation models, such as WACCM-X, can provide insight into smaller-scale structures in the equatorial ionosphere. This represents a new application of such models, enabling

247 potential future investigations focused on understanding, for example, the day-to-day
 248 variability of 150-km echoes.

249 The effect of the solar flare on the equatorial vertical plasma drifts was also investi-
 250 gated. The JRO observations show a sudden decrease in vertical plasma drift veloc-
 251 ity of $15\text{-}20\text{ ms}^{-1}$ after the onset of the solar flare. The WACCM-X simulations repro-
 252 duce a decrease in vertical plasma drift at 320°E geographic longitude, but only a weak
 253 ($1\text{-}2\text{ ms}^{-1}$) decrease at the longitude of Jicamarca (285°E). The vertical plasma drift changes
 254 are attributed to changes in the conductivity in the simulations, which changes the day-
 255 time eastward electric field, and the longitudinal differences may be related to differences
 256 in the zonal winds at the time of the solar flare. This demonstrates that simulating the
 257 electrodynamic effects of solar flares requires accurately simulating both the zonal winds
 258 as well as the conductivities.

259 Acknowledgments

260 WACCM-X is part of the Community Earth System Model (CESM) and the source code
 261 is available at <http://www.cesm.ucar.edu>. The WACCM-X simulation output, and Ji-
 262 camarca SNR observations, used in this publication are available at <https://doi.org/10.26024/ahcm-6d40>. The GOES x-ray observations are available from NASA NCEI (<https://www.ngdc.noaa.gov/stp/satellite/goes/>). We would like to acknowledge high-performance computing support from Cheyenne (doi:10.5065/D6RX99HX) provided by NCARs Computational and Information Systems Laboratory. This mate-
 263 rial is based upon work supported by the National Center for Atmospheric Research, which
 264 is a major facility sponsored by the National Science Foundation under Cooperative Agree-
 265 ment No. 1852977. We thank the International Space Science Institute for facilitating
 266 discussions related to this paper as part of the International Team "An Exploration of
 267 the Valley Region in the Low Latitude Ionosphere: Response to Forcing from Below and
 268 Above and Relevance to Space Weather". The participation of J. L. C. in this work is
 269 part of the project supported by the Deutsche Forschungsgemeinschaft (DFG, German
 270 Research Foundation) under SPP 1788 (DynamicEarth)-CH 1482/1-2 (DYNAMITE2).

274 References

275 Annadurai, N. M. N., Hamid, N. S. A., Yamazaki, Y., & Yoshikawa, A. (2018). (2018).
 276 Investigation of Unusual Solar Flare Effect on the Global Ionospheric Cur-
 277 rent System. *J. Geophys. Res. Sp. Phys.*, *123*(10), 8599–8609. doi:
 278 [10.1029/2018JA025601](https://doi.org/10.1029/2018JA025601)

279 Balsley, B. B. (1964). Evidence of a stratified echoing region at 150 kilometers in
 280 the vicinity of the magnetic equator during daylight hours. *J. Geophys. Res.*,
 281 *69*(9), 1925–1930. doi: [10.1029/JZ069i009p01925](https://doi.org/10.1029/JZ069i009p01925)

282 Chamberlin, P. C., Woods, T. N., & Eparvier, F. G. (2008). Flare Irradiance Spec-
 283 tral Model (FISM): Flare component algorithms and results. *Sp. Weather*,
 284 *6*(5). doi: [10.1029/2007SW000372](https://doi.org/10.1029/2007SW000372)

285 Chau, J., Woodman, R., Milla, M., & Kudeki, E. (2009). Naturally enhanced ion-
 286 line spectra around the equatorial 150-km region. *Ann. Geophys.*, *27*, 933–942.

287 Chau, J. L. (2004). Unexpected spectral characteristics of VHF radar signals from
 288 150-km region over Jicamarca. , *31*, L23803, doi:[10.1029/2004GL021620](https://doi.org/10.1029/2004GL021620).

289 Chau, J. L., & Kudeki, E. (2006). Statistics of 150-km echoes over Jicamarca based
 290 on low-power VHF observations. *Ann. Geophys.*, *24*(5), 1305–1310. doi: [10.5194/angeo-24-1305-2006](https://doi.org/10.5194/angeo-24-1305-2006)

291 Chau, J. L., & Kudeki, E. (2013). Discovery of two distinct types of equatorial
 292 150 km radar echoes. *Geophysical Research Letters*, *40*(17), 4509–4514.
 293 Retrieved from <https://agupubs.onlinelibrary.wiley.com/doi/abs/10.1002/grl.50893> doi: [10.1002/grl.50893](https://doi.org/10.1002/grl.50893)

294 Chau, J. L., Kudeki, E., & Milla, M. (2009). Multi-frequency radar studies of the
 295 equatorial 150-km region. In N. Swarnalingam & W. K. Hocking (Eds.), *Pro-*

298 *ceedings of the 12th international symposium on equatorial aeronomy* (p. 165-
 299 168). London, Ontario, Canada.

300 Choudhary, R. K., St.-Maurice, J.-P., & Mahajan, K. K. (2004). Observation
 301 of coherent echoes with narrow spectra near 150 km altitude during
 302 daytime away from the dip equator. *Geophys. Res. Lett.*, 31(19). doi:
 303 10.1029/2004GL020299

304 de Paula, E. R., & Hysell, D. L. (2004). The São Luís 30 MHz coherent scatter
 305 ionospheric radar: System description and initial results. *Radio Sci.*, 39(1).
 306 Retrieved from <https://agupubs.onlinelibrary.wiley.com/doi/abs/10.1029/2003RS002914> doi: 10.1029/2003RS002914

307 Gelaro, R., McCarty, W., Suárez, M. J., Todling, R., Molod, A., Takacs, L., ...
 308 Zhao, B. (2017). The Modern-Era Retrospective Analysis for Research and
 309 Applications, Version 2 (MERRA-2). *J. Clim.*, 30(14), 5419-5454. doi:
 310 10.1175/JCLI-D-16-0758.1

311 Heelis, R. A., Lowell, J. K., & Spiro, R. W. (1982). A model of the high-latitude
 312 ionospheric convection pattern. *J. Geophys. Res. Sp. Phys.*, 87(A8), 6339-
 313 6345. doi: 10.1029/JA087iA08p06339

314 Kudeki, E., & Fawcett, C. D. (1993). High resolution observations of 150
 315 km echoes at Jicamarca. *Geophys. Res. Lett.*, 20(18), 1987-1990. doi:
 316 10.1029/93GL01256

317 Kudeki, E., Fawcett, C. D., Ecklund, W. L., Johnston, P. E., & Franke, S. J. (1998).
 318 Equatorial 150-km irregularities observed at Pohnpei. *Geophys. Res. Lett.*,
 319 25(21), 4079-4082. doi: 10.1029/1998GL900069

320 Lehmacher, G., Lu, X., Kudeki, E., Reyes, P. M., & Milla, M. (2018, May). Si-
 321 multaneous observations of 150-km echoes and ionosonde virtual heights at
 322 jicamarca. In *Proceedings of the 12th international workshop on technical and*
 323 *scientific aspects of mst radar*. Ahmedabad, India.

324 Lehmacher, G. A., Kudeki, E., Akgiray, A., Guo, L., Reyes, P., & Chau, J. (2009).
 325 Radar cross sections for mesospheric echoes at jicamarca. *Annales Geophysi-
 326 cae*, 27(7), 2675-2684. Retrieved from <https://www.ann-geophys.net/27/2675/2009/> doi: 10.5194/angeo-27-2675-2009

327 Lehmacher, G. A., Kudeki, E., Reyes, P. M., Lee, K., Heale, C. J., & Snively, J. B.
 328 (2019). Gravity wave ducting observed in the mesosphere over jicamarca,
 329 peru. *Journal of Geophysical Research: Atmospheres*, 124(10), 5166-5177.
 330 Retrieved from <https://agupubs.onlinelibrary.wiley.com/doi/abs/10.1029/2019JD030264> doi: 10.1029/2019JD030264

331 Liu, H.-L., Bardeen, C. G., Foster, B. T., Lauritzen, P., Liu, J., Lu, G., ... Wang,
 332 W. (2018). Development and Validation of the Whole Atmosphere Community
 333 Climate Model With Thermosphere and Ionosphere Extension (WACCM-X
 334 2.0). *J. Adv. Model. Earth Syst.*, 10(2), 381-402. doi: 10.1002/2017MS001232

335 Liu, J., Liu, H., Wang, W., Burns, A. G., Wu, Q., Gan, Q., ... Schreiner, W. S.
 336 (2018). First Results From the Ionospheric Extension of WACCM-X During
 337 the Deep Solar Minimum Year of 2008. *J. Geophys. Res. Sp. Phys.*, 123(2),
 338 1534-1553. doi: 10.1002/2017JA025010

339 Marsh, D. R., Mills, M. J., Kinnison, D. E., Lamarque, J. F., Calvo, N., &
 340 Polvani, L. M. (2013). Climate change from 1850 to 2005 simulated in
 341 CESM1(WACCM). *J. Clim.*. doi: 10.1175/JCLI-D-12-00558.1

342 Neale, R. B., Richter, J., Park, S., Lauritzen, P. H., Vavrus, S. J., Rasch, P. J.,
 343 & Zhang, M. (2013). The Mean Climate of the Community Atmosphere
 344 Model (CAM4) in Forced SST and Fully Coupled Experiments. *J. Clim.*. doi:
 345 10.1175/JCLI-D-12-00236.1

346 Oppenheim, M. M., & Dimant, Y. S. (2016). Photoelectron-induced waves: A likely
 347 source of 150 km radar echoes and enhanced electron modes. *Geophys. Res.
 348 Lett.*, 43(8), 3637-3644. doi: 10.1002/2016GL068179

349 Patra, A., Pavan Chaitanya, P., St-Maurice, J.-P., Otsuka, Y., Yokoyama, T., & Ya-

353 mamoto, M. (2017). The solar flux dependence of ionospheric 150 km radar
 354 echoes and implications. *Geophysical Research Letters*, 44(22).

355 Patra, A. K., Pavan Chaitanya, P., & Tiwari, D. (2011). Characteristics of 150
 356 km echoes linked with solar eclipse and their implications to the echoing phe-
 357 nomenon. *J. Geophys. Res. Sp. Phys.*, 116(A5). doi: 10.1029/2010JA016258

358 Patra, A. K., Yokoyama, T., Otsuka, Y., & Yamamoto, M. (2008). Daytime 150-km
 359 echoes observed with the Equatorial Atmosphere Radar in Indonesia: First
 360 results. *Geophys. Res. Lett.*, 35(6). doi: 10.1029/2007GL033130

361 Perkins, F., Salpeter, E., & Yngvesson, K. (1965). Incoherent scatter from plasma
 362 oscillations in the ionosphere. *Physical Review Letters*, 14(15), 579.

363 Pettit, J., Randall, C. E., Marsh, D. R., Bardeen, C. G., Qian, L., Jackman, C. H.,
 364 ... Harvey, V. L. (2018). Effects of the September 2005 Solar Flares and Solar
 365 Proton Events on the Middle Atmosphere in WACCM. *J. Geophys. Res. Sp. Phys.*
 366 doi: 10.1029/2018JA025294

367 Qian, L., Burns, A. G., Chamberlin, P. C., & Solomon, S. C. (2011). Variability
 368 of thermosphere and ionosphere responses to solar flares. *J. Geophys. Res. Sp.*
 369 *Phys.*, 116(A10). doi: 10.1029/2011JA016777

370 Qian, L., Burns, A. G., Solomon, S. C., & Chamberlin, P. C. (2012). Solar flare im-
 371 pacts on ionospheric electrodynamics. *Geophys. Res. Lett.*, 39(6). doi: 10.1029/
 372 2012GL051102

373 Reyes, P. (2012). *Solar Flare Effects Observed Over Jicamarca During MST-ISR*
 374 *Experiments* (Master of Science, University of Illinois at Urbana-Champaign).
 375 Retrieved from <http://hdl.handle.net/2142/31196>

376 Reyes, P. (2017). *Study of Waves Observed in the Equatorial Ionospheric Val-*
 377 *ley Region using Jicamarca ISR and VIPIR Ionosonde* (Doctor of Phi-
 378 *losophy, University of Illinois at Urbana-Champaign*). Retrieved from
 379 <http://hdl.handle.net/2142/98349>

380 Richmond, A. D., Ridley, E. C., & Roble, R. G. (1992). A thermosphere/ionosphere
 381 general circulation model with coupled electrodynamics. *Geophys. Res. Lett.*,
 382 19(6), 601–604. doi: 10.1029/92GL00401

383 Roble, R. G., Ridley, E. C., Richmond, A. D., & Dickinson, R. E. (1988). A cou-
 384 pled thermosphere/ionosphere general circulation model. *Geophys. Res. Lett.*,
 385 15(12), 1325–1328. doi: 10.1029/GL015i012p01325

386 Smith, A. K., Pedatella, N. M., Marsh, D. R., & Matsuo, T. (2017). On the Dynam-
 387 ical Control of the MesosphereLower Thermosphere by the Lower and Middle
 388 Atmosphere. *J. Atmos. Sci.*, 74(3), 933–947. doi: 10.1175/JAS-D-16-0226.1

389 Tsunoda, R. T., & Ecklund, W. L. (2008). On the sheet-like nature of 150 km (F1)
 390 radar echoes. *Geophys. Res. Lett.*, 35(5). doi: 10.1029/2007GL032152

391 Zhang, R., Liu, L., Le, H., & Chen, Y. (2017). Equatorial ionospheric electrodynam-
 392 ics during solar flares. *Geophys. Res. Lett.*, 44(10), 4558–4565. doi: 10.1002/
 393 2017GL073238